Journal of
Materials Chemistry B

Materials for biology and medicine

www.rsc.org/MaterialsB

ROYAL SOCIETY
OF CHEMISTRY

PAPER
Kai A. I. Zhang *et al.*
Enhanced visible light promoted antibacterial efficiency of conjugated
microporous polymer nanoparticles *via* molecular doping

175 YEARS

Enhanced visible light promoted antibacterial efficiency of conjugated microporous polymer nanoparticles *via* molecular doping†

Beatriz Chiyin Ma, Saman Ghasimi, Katharina Landfester and Kai A. I. Zhang*

The increase in the resistance of bacteria to antibiotics is one of the main concerns of public health and holds a great demand in the development of new disinfection methods. Photodynamic therapy (PDT) has been considered as a promising alternative approach towards the eradication of bacteria and great attention has been dedicated to the use of non-toxic and pure organic PDT agents. Herein we report the structural design method of a series of conjugated microporous polymer nanoparticles (CMP NPs) as a new class of highly effective photoactive materials for the inactivation of bacteria in water upon visible light exposure. Through molecular doping of electron-withdrawing moieties into electron-donating polymer backbones, enhanced antibacterial properties are demonstrated upon the inactivation of *Escherichia coli* K-12 and *Bacillus subtilis* mainly by means of photogeneration of singlet oxygen as the main photogenerated active species. Additionally, the high stability, reusability and disinfection mechanism of the CMP NPs are also described.

Introduction

The emergence of multi-resistant bacteria against antibiotics is considered to be one of the main challenges in modern public healthcare.[1–5] In recent years, antibacterial photodynamic therapy (PDT) holds great promise as an alternative approach to the disinfection of bacteria. In comparison to conventional inactivation methods, PDT presents the advantage of not inducing the selection of resistant strains since its mode of action is based on the generation of reactive oxygen species (ROS) upon light irradiation.[6,7]

Recently, a range of inorganic or metalloorganic semiconductor photocatalysts primary based on TiO_2,[8,9] porphyrin derivatives and other metal-based complexes have been developed as suitable materials for disinfection.[6,10,11] Besides these metal-containing active systems, recent studies have reported the development of pure organic and metal-free semiconductors based on water soluble conjugated polymers with visible light induced antibacterial properties.[12–16] Considerable efforts have been focused on the development of photoactive nanomaterials towards bacterial disinfection,[17] since they offer great advantages due to their surface to volume ratio.[18] However, only a few examples of the employment of non-metal based nanostructured photoactive systems were reported.[8] It is therefore of great benefit

Max Planck Institute for Polymer Research, Ackermannweg 10, D-55128 Mainz, Germany. E-mail: kai.zhang@mpip-mainz.mpg.de
† Electronic supplementary information (ESI) available. See DOI: 10.1039/c6tb00943c

to further develop a new class of metal-free photoactive systems with broad light absorption range, high efficiency and stability.

Conjugated microporous polymers (CMPs), a class of semiconductive porous organic materials with the combination of photoactive π-conjugated backbone and microporosity,[19,20] have recently emerged as stable heterogeneous photocatalysts for organic syntheses and especially photo-redox reactions under visible light irradiation.[21–24] Previous works have shown that conjugated microporous polymers were able to generate active oxygen species such as superoxide ($^{\bullet}O_2^-$) and singlet oxygen ($^1O_2$) under visible light irradiation.[25–28] Especially singlet oxygen is well known as the main reactive oxygen species responsible for cell death in antimicrobial photodynamic therapy.[29–31]

Besides the material class choice perspective, there are a vast number of useful structural modification methods of semiconductor-based materials in order to enhance the pristine functionalities. Among them, the introduction of foreign impurities into a semiconductor, the so-called doping method, has been largely employed as an efficient strategy to manipulate the electronic structure of semiconductors, and thus, to achieve the desired control over the optical, conductive, magnetic or other physical properties for targeted applications.[9,32]

Here in the present work, we report the use of a series of conjugated microporous polymer nanoparticles (CMP NPs) as a new class of highly efficient metal-free photocatalysts for visible light promoted antibacterial PDT. Taking the doping method for traditional semiconductors as a role model, a structural design principle *via* molecular doping of an electron-withdrawing

moiety, benzothiadiazole unit (BT), into the backbone of the pure organic polymer network containing only the electron-donating thiophene units was introduced in order to modify the ability for the generation of active oxygen species. An enhanced disinfection effect on *Escherichia coli* K-12 under visible light irradiation was demonstrated as the model system.

Results and discussion

The conjugated microporous polymer nanoparticles (CMP NPs) were prepared *via* a palladium-catalysed Sonogashira–Hagihara cross-coupling polycondensation reaction in an oil-in-water mini emulsion.[25,33] In particular, as illustrated in Scheme 1, the electron-donating thiophene unit-based (Th) polymer network Th-BT-0 was taken as the pristine polymer backbone structure. *Via* successive doping of the electron-withdrawing benzothiadiazole (BT) unit, into the polymer backbone, a series of CMP NPs were obtained containing different chemical compositions. The detailed synthesis and characterization of the polymers are described in the Experimental section and in the ESI.†

Fig. 1 shows the SEM and TEM images of the CMP NPs. A variety of morphologies ranging from nanospheres, nanorods to nanorings were observed. Th-BT-0 and Th-BT-25 were formed as nanospheres with a diameter of *ca.* 180 nm, whereas the Th-BT-50 appeared as "worm-like" nanoparticles with a length of *ca.* 250 nm, which could be a transitional state between nanospheres and ring-shaped nanostructures exhibited by Th-BT-70, Th-BT-90 and Th-BT-100. The latter was in accordance with our previous report.[25] The morphological trend might indicate that the shape variation depends on the addition of the BT unit and the increasing amount of the strong acceptor unit possibly pushed the structure towards a ring formation due to strong π–π stacking at the interface during the miniemulsion polymerization.[25]

Solid-state magic angle spinning nuclear magnetic resonance (^{13}C/MAS NMR) spectroscopy showed typical chemical shifts between 120 and 150 ppm for all CMP NPs, which can be

assigned to the aromatic rings in the polymer backbone (Fig. S1–S6, ESI†). For Th-BT-25, Th-BT-50, Th-BT-70, Th-BT-90 and Th-BT-100 containing benzothiadiazole moieties, a clear trend of increasing signals at about 155 ppm could be observed, which can be assigned to the adjacent carbon next to nitrogen in the BT unit, indicating an increase of the BT content in the polymer backbone structure.

The FT-IR spectra of the polymers (Fig. S7, ESI†) showed characteristic vibrational peaks at about 2250–2100 cm^{-1}, which corresponded to the triple bonds. A distinctive vibrational peak at about 840 cm^{-1} is assigned to the N–S deformation band of the BT unit on Th-BT-25, Th-BT-50, Th-BT-70, Th-BT-90 and Th-BT-100, and absent on Th-BT-0. At the same time, vibrational peaks at about 1196 cm^{-1} and 791 cm^{-1} are attributed to the thiophene units on Th-BT-0, Th-BT-25, Th-BT-50, Th-BT-70, Th-BT-90 and absent on Th-BT-100 (Fig. S7, ESI†). Thermogravimetric analysis (TGA) indicated that all CMP NPs are thermally stable up to 300 °C, with Th-BT-0, which contains only thiophene units, exhibiting the largest weight loss among all of CMP NPs (Fig. S8, ESI†). It is worth noticing that the high weight content (about 75%) after heating the samples to 1000 °C could indicate the formation of carbonized materials containing sulphur and nitrogen.

The porosities of the CMP NPs were investigated by nitrogen adsorption/desorption experiments at 77.3 K (for details, see Experimental section), the data are listed in Table 1. All CMP NPs showed a typical Type I adsorption isotherm (Fig. S9 and S10, ESI†), which indicates a predominant microporous structure. The Brunauer–Emmett–Teller (BET) surface areas of the polymers varied from 129 to 319 m^2 g^{-1}, with Th-BT-100 exhibiting the highest BET surface area in the polymer series. A similar pore diameter (1.5 nm) was obtained for all CMP NPs (Table 1).

The UV/Vis absorption spectra of CMP NPs are displayed in Fig. 2a. A clear trend in the absorption range among the polymers could be observed. The only donor-based Th-BT-0 showed the broadest absorption range in the visible light region. Through the successive addition of increasing amounts of the BT unit into the polymer backbone, the absorption range of the polymers became sharper towards the blue region of the spectrum. This indicates increasing HOMO–LUMO band gaps with the addition of more electron-withdrawing moieties into the polymer backbone. All polymers showed a similar fluorescence emission range from 400 and 800 nm, with a peak at about 540 nm (Fig. S11, ESI†). However, it can be seen that with the increase in the content of BT units, a progressive decrease in the fluorescence intensity was observed.

To further study the electronic properties of the polymers, cyclic voltammetry (CV) measurements were conducted to determine the valence band (VB) and the conduction band (CB) positions. The CV data are displayed in Fig. 2b. Significantly, a clear tendency for the expansion of the band gaps of the polymer series was observed *via* continuous addition of the electron-withdrawing BT units into the thiophene-based polymer network backbone. This result corresponds to the narrowing tendency observed in the UV/Vis absorption range of the polymers. Th-BT-100, which only contains BT, exhibited the broadest band
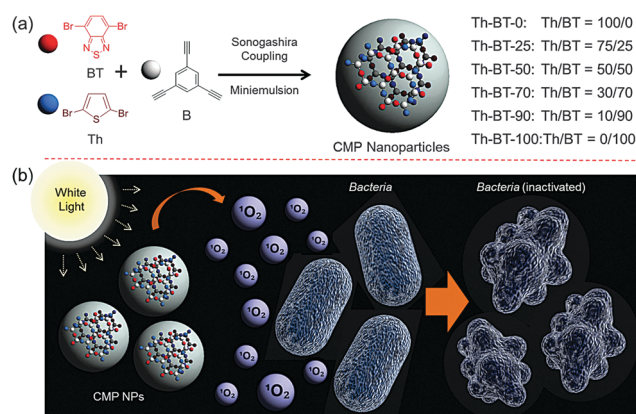
Scheme 1 (a) Illustrated structures and synthetic route to the conjugated microporous polymer nanoparticles (CMP NPs) *via* Sonogashira–Hagihara cross-coupling reaction *via* miniemulsion polymerization and the ratios of the monomer moieties in the polymer backbones. (b) Schematic representation of the mechanism for the inactivation of bacteria using CMP NPs.
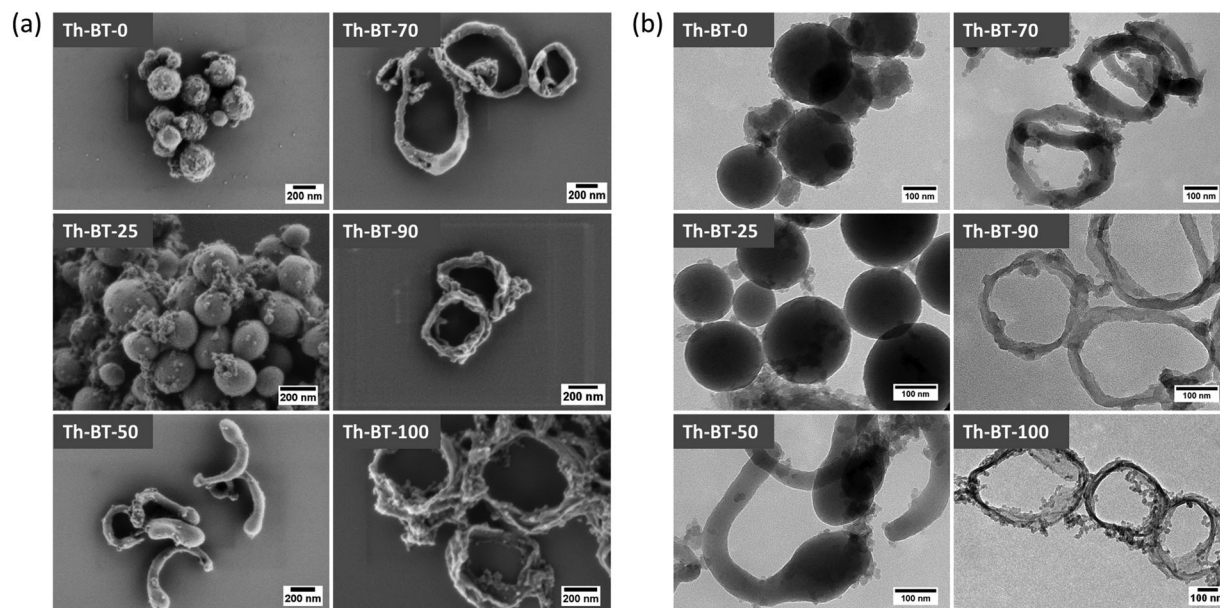
This journal is © The Royal Society of Chemistry 2016

J. Mater. Chem. B, 2016, **4**, 5112–5118 | **5113**

Fig. 1 (a) SEM and (b) TEM images of the CMP NPs.

Table 1 Porosity data of CMP NPs

CMP NPs	Surface area[a] [$m^2\ g^{-1}$]	Pore volume[b] [$cm^3\ g^{-1}$]	Pore diameter [nm]
Th-BT-0	145	0.19	1.5
Th-BT-25	226	0.33	1.5
Th-BT-50	129	0.18	1.5
Th-BT-70	250	0.41	1.5
Th-BT-90	199	0.39	1.5
Th-BT-100	319	0.60	1.4

[a] BET surface area calculated over the pressure range 0.05–0.35 P/P_0.
[b] Pore volume calculated at $P/P_0 = 0.99$.

Fig. 2 (a) UV/Vis absorption spectra and (b) valence band (VB) and conduction band (CB) positions of the CMP NPs.

gap of 2.51 eV with the VB and CB positions lying at +1.61 V and −0.90 V, indicating the highest redox potential of the material. In contrast, the only thiophene containing polymer Th-BT-0 exhibited the narrowest band gap of 1.71 eV with the VB and CB positions lying at +1.09 V and −0.62 V, respectively.

According to the aforementioned ability of conjugated microporous polymers in generating active oxygen species, we then conducted electron paramagnetic resonance (EPR) spin trapping experiments using 2,2,6,6-tetramethylpiperidine (TEMP) and 5,5-dimethyl-1-pyrroline N-oxide (DMPO) as singlet oxygen ($^1O_2$) and superoxide ($^\bullet O_2^-$) trapping agents, respectively.[34,35] As displayed in Fig. 3a, 2,6,6,6-tetramethylpiperidinyloxyl (TEMPO-$^1O_2$) adducts could be determined by using all the CMP nanoparticles under visible light irradiation. A clear tendency can be seen for the increment of the TEMPO-$^1O_2$ signal intensity by using the CMP NPs containing increasing contents of BT units in the polymer backbone and Th-BT-100 was able to generate the most intense TEMPO-$^1O_2$ signals among all the polymer series. This result suggests its superior capacity to photogenerate $^1O_2$. It was also observed that weak DMPO-$^\bullet O_2^-$ signals could be found in the experiments under light and dark conditions, which indicates that only a minimal
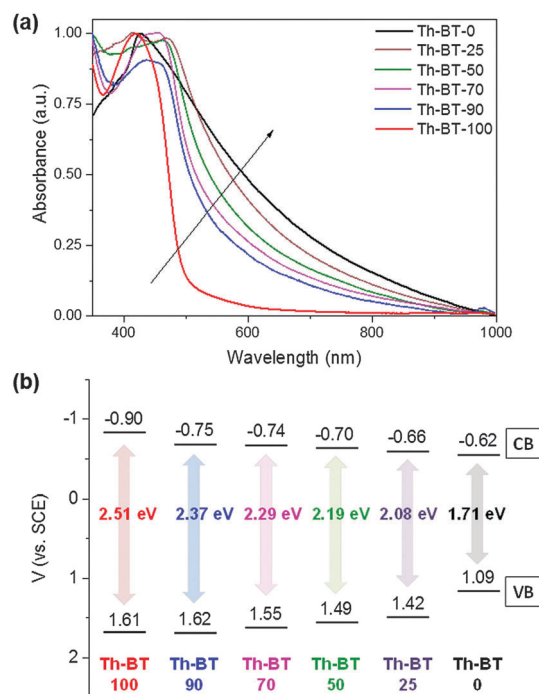
amount of $^\bullet O_2^-$ could be generated by the CMP NPs under visible light irradiation (Fig. S12b, ESI†). Nevertheless, these results further demonstrate that Th-BT-100 with the highest redox potential was indeed the most efficient photocatalyst among all the series of polymers.

The visible light promoted antibacterial disinfection ability of the CMP NPs were evaluated using *Escherichia coli* K-12 and *Bacillus subtilis* as Gram negative and Gram positive model
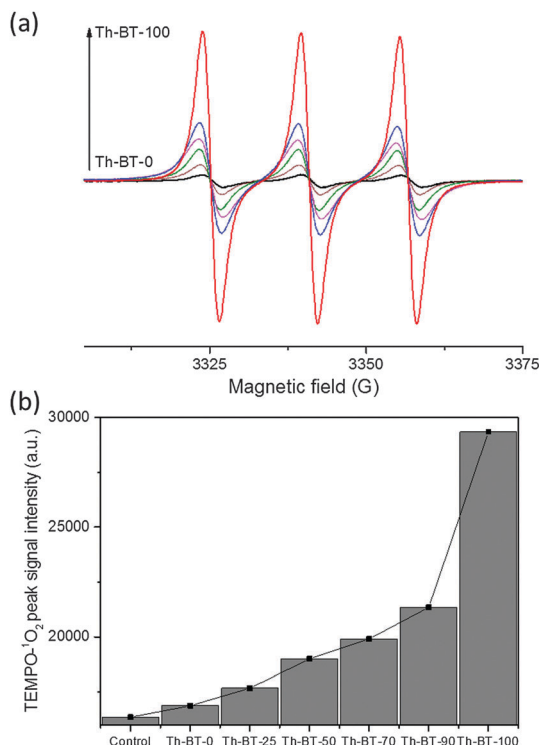
5114 | J. Mater. Chem. B, 2016, 4, 5112–5118

This journal is © The Royal Society of Chemistry 2016

Fig. 3 (a) Electron paramagnetic resonance (EPR) spin trapping spectra of TEMPO-$^1O_2$ adducts in acetonitrile generated by different CMP NPs under visible light irradiation. Conditions: CMP NPs (1 mg mL^{-1}), 2,2,6,6-tetramethylpiperidine (0.1 M), 2 h white light irradiation, room temperature. (b) Difference between peak signal intensities of the TEMPO-$^1O_2$ adducts for the CMP NPs after visible light exposure.

systems, respectively. In this study, a suspension of bacteria was incubated with CMP NPs and exposed to white light irradiation for different time intervals. The viability of the bacteria was assessed using the standard plating method (see the Experimental section for details). To note, all CMP NPs showed no toxic effects on bacteria cells in the absence of light irradiation as shown in the dark experiment (Fig. S13, ESI†). Fig. 4a summarizes the results of the antibacterial activity of all CMP NPs against *E. coli* K-12 under visible light irradiation. It could be clearly seen that the inactivation efficiency of the CMP NPs could be enhanced progressively by increasing the BT content in the polymer backbone, with Th-BT-100 as the most efficient antibacterial agent within the polymer series, achieving about 95% cell death after 120 min of visible light irradiation. This is comparable with well-known non-metal based photocatalysts reported recently.[35] Additionally, compared to its bulk-made form, Th-BT-100 as nanoparticles showed also significant higher antibacterial efficiency (Fig. S14, ESI†). This result is in accordance with previous works in which nanoparticulate systems showed enhanced photocatalytic activity in contrast to the bulk material.[25]

Th-BT-100 also showed high disinfection efficiency against *B. subtilis* (Fig. 4b), reaching about 97% of cell death after 120 min of visible light irradiation, which indicates that Th-BT-100 is highly effective in inactivating both Gram negative and Gram positive bacteria. The scanning electron microscopy (SEM) and

photographs of *E. coli* K-12 and *B. subtilis* cells and colonies in the control, dark and light-induced antimicrobial experiments are shown in Fig. 4c. It can be clearly seen that no microstructural changes of the bacteria cells can be observed either in the control experiment (top), without Th-BT-100 as an antibacterial agent and in the absence of light irradiation, or in the presence of Th-BT-100 in the dark (middle). In comparison, by using Th-BT-100 under visible light exposure as an antibacterial agent, morphological changes with severe disruptions of the cell membrane of *E. coli* K-12 and *B. subtilis* were observed (bottom), which resulted in further release of the cell content and cell death. These results indicate that the inactivation process of the bacteria is caused by the photocatalytic effect of the CMP NPs under light irradiation.

Previous studies showed that CMP NPs could be used for the photodegradation of organic dyes in water under visible light irradiation.[25] A number of reactive species such as superoxide ($^\bullet O_2^-$), singlet oxygen ($^1O_2$), electron (e^-), photo-generated hole (h^+) or hydrogen peroxide (H_2O_2) played important roles in the photocatalytic process.[8,11] In order to further understand the mechanism of the antimicrobial effect of the CMP NPs, we conducted a series of control experiments with the addition of different active species scavengers into the bacteria reaction system. In particular, ammonium oxalate (AO), catalase, NaNO$_3$ and TEMP were introduced as scavengers for h^+, H_2O_2, e^- and $^1O_2$, respectively. Vitamin C was also used as a general radical scavenger. It is important to mention that the concentration of each scavenger was adjusted to ensure the highest scavenging effect without presenting toxicity on *E. coli* K-12 (Fig. S15, ESI†).[9,11]

The effects of different scavengers are illustrated in Fig. 5a. It can be seen that without the addition of any scavenger, nearly 95% of the *E. coli* K-12 were inactivated after 120 min of light irradiation. *Via* the addition of TEMP, a singlet oxygen scavenger, the survival rate of *E. coli* K-12 dropped only about 30%, which confirms the superior role of $^1O_2$ in the photo-inactivation process of the bacteria. The addition of NaNO$_3$ as a general electron scavenger showed an effect similar to TEMP, which suggests that once the electron is trapped it will no longer be able to transfer its energy to dioxygen, and therefore blocking the generation of $^1O_2$. Interestingly, the addition of AO as the hole scavenger led to about 60% of bacteria survival, which indicates that Th-BT-100 was not only able to promote photocatalytic bacterial disinfection *via* the reduction of molecular oxygen, but also *via* a direct oxidative pathway from the photo-generated electron–hole species, which could likely oxidize the components of the cell membrane of *E. coli* K-12 and subsequently leading to its direct inactivation and possible mineralization of its organic content.[36,37] As shown in Fig. 4c, the bacteria cells were surrounded by the nanoparticles; this proximity was important for an enhanced diffusion of the active species from the nanoparticles onto the bacteria cells despite the short lifetime of $^1O_2$ in water.[38,39]

To further study the $^1O_2$ generation efficiency, an additional experiment was performed using α-terpinene as the $^1O_2$ trapping agent.[9,11] A full conversion of ascaridole as a product after 2 h under visible light irradiation using Th-BT-100 as a photocatalyst
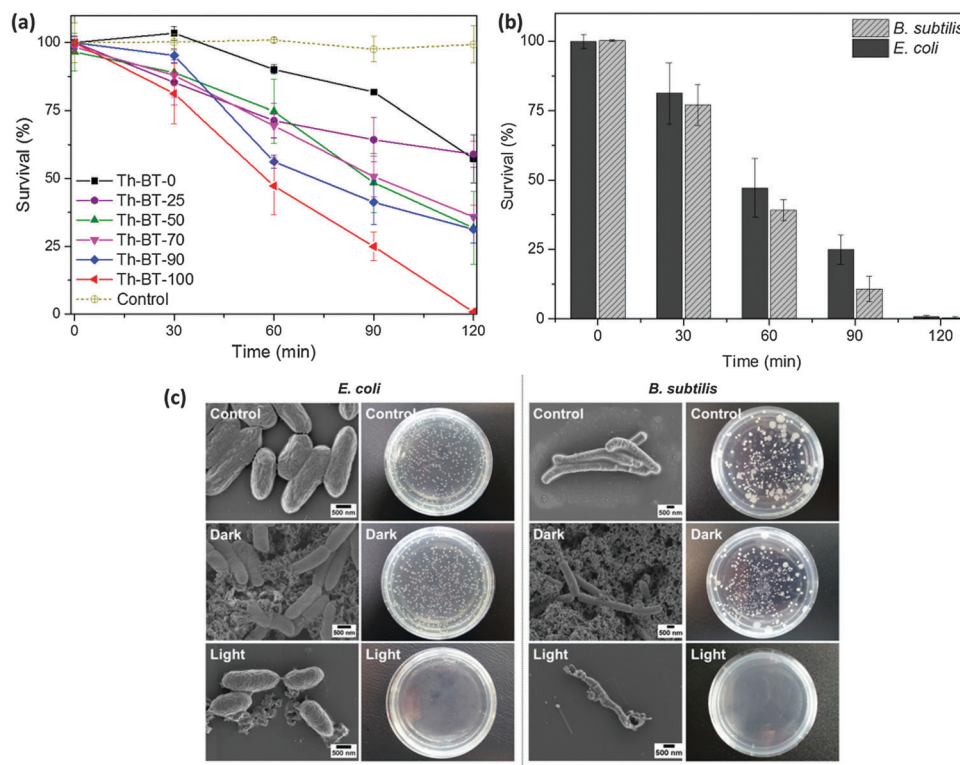
Fig. 4 (a) Photocatalytic inactivation of *E. coli* K-12 in the presence of different CMP NPs (1 mg mL^{-1}) under visible light irradiation. Data represent the results of three independent experiments (mean ± standard error of the mean). (b) Photocatalytic inactivation of *E. coli* K-12 and *B. subtilis* in the presence of Th-BT-100 (1 mg mL^{-1}) under visible light irradiation. Data represent the results of three independent experiments (mean ± standard error of the mean). (c) SEM images and photographs of *E. coli* K-12 and *B. subtilis* colonies on agar plate as a control group in the absence of Th-BT-100 and light irradiation (top); treated with BT-100 in the dark (middle); and after 120 min of visible light irradiation (bottom).

was observed (Fig. S16 and S17, ESI†), giving an $^1O_2$ generation rate of *ca.* 0.14 mmol g^{-1} s^{-1} for Th-BT-100.

Furthermore, the stability and reusability of Th-BT-100 were investigated *via* repeated experiments under the same reaction conditions. As shown in Fig. 5b, Th-BT-100 could be reused for another three additional cycles and nearly 95% of bacteria were inactivated in each cycle. No apparent changes were observed in the FT-IR spectra of Th-BT-100 after the photocatalytic reaction, which indicates the high stability of the photocatalyst (Fig. S19, ESI†). And it is worth pointing out that a longer irradiation time (4 h) did not affect the photoactivity of the polymer nanoparticles (Fig. S20, ESI†).

Conclusions

In conclusion, we reported a structural design principle of the conjugated microporous polymer nanoparticles as a new class of highly effective photoactive agents for the inactivation of bacteria in water under visible light irradiation. *Via* a molecular doping method of electron-withdrawing moieties into the electron-donating polymer backbone, enhanced light-induced antimicrobial activity could be demonstrated in the photo-inactivation of *E. coli* K-12 and *B. subtilis*. Different photo-generated active species could be determined using the polymer nanoparticles, with singlet oxygen playing the main role during

the photo-inactivation process. This study demonstrated a further application of conjugated microporous polymer nanoparticles as pure organic, non-toxic and active agents for the photodynamic inactivation of microorganisms.

Experimental section

Materials

1,3,5-Triethynylbenzene (97%), 2,5-dibromothiophene (96%), copper(I) iodide (99%), tetrakis(triphenylphosphine) palladium(0) (99%), potassium carbonate (K_2CO_3) (99%), ammonium oxalate (99%), catalase, sodium nitrate (99%), L-ascorbic acid (99%), triethylamine (99%), 5,5-dimethyl-1-pyrroline *N*-oxide (97%), 2,2,6,6-tetramethylpiperidine (98%), 5,5-dimethyl-1-pyrroline *N*-oxide (97%), α-terpinene (90%), mesitylene (98%) and all other solvents were purchased from Sigma Aldrich. Sodium *n*-dodecyl-sulfate (99%) was obtained from Alfa Aesar. 4,7-Dibromobenzo[*c*]-1,2,5-thiadiazole (97%) was purchased from Combi Blocks. *Escherichia coli* K-12 and *Bacillus subtilis* were purchased from DSMZ Leibniz-Institute (Braunschweig, Germany). All chemicals and solvents were used as received unless otherwise specified.

Synthesis of CMP NPs

The synthesis of CMP nanoparticles was performed using the Sonogashira–Hagihara cross coupling reaction *via* oil-in-water
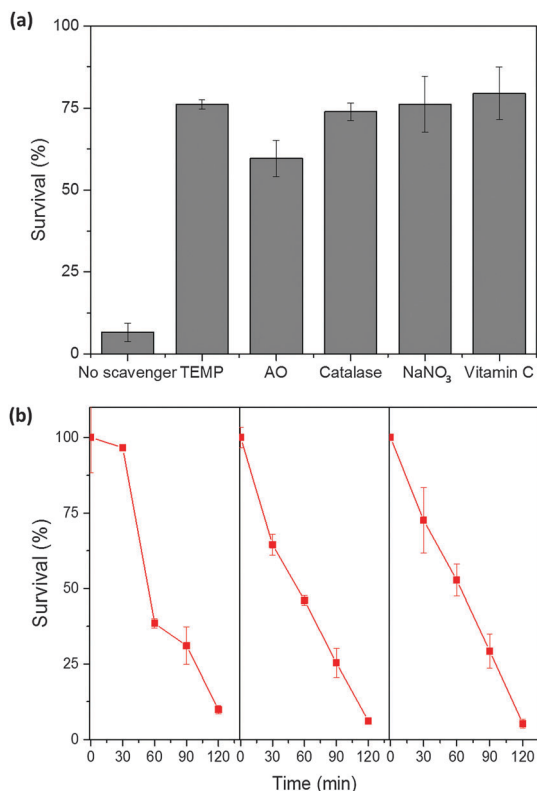
Fig. 5 (a) Photocatalytic inactivation of *E. coli* K-12 using different scavengers (ammonium oxalate (AO), catalase, $NaNO_3$, TEMP and vitamin C) and Th-BT-100 as an antibacterial agent. Conditions: 0.05 mmol L^{-1} concentration of scavengers, air, 120 min white light irradiation. Data represent the results of three independent experiments (mean ± standard error of the mean). (b) Repeated experiments of photocatalytic inactivation of *E. coli* K-12 (3×10^6 cfu mL^{-1}) in the presence of Th-BT-100 (1 mg mL^{-1}) under visible light irradiation. Data represent the results of three independent experiments (mean ± standard error of the mean).

miniemulsion polymerization. 1,3,5-Triethynylbenzene (50 mg), tetrakis(triphenylphosphine) palladium(0) (19.24 mg), and copper(I) iodide (3.24 mg) were dissolved in 2 mL of toluene. Then, increasing amounts of 4,7-dibromobenzo[*c*]-1,2,5-thiadiazole and decreasing amounts of 2,5-dibromothiophene were added to the mixture in each reaction as follows: Th-BT-0 (2,5-dibromothiophene: 120.96 mg), Th-BT-25 (2,5-dibromothiophene: 90.72 mg; 4,7-dibromobenzo[*c*]-1,2,5-thiadiazole: 36.75 mg), Th-BT-50 (2,5-dibromothiophene: 60.48 mg; 4,7-dibromobenzo[*c*]-1,2,5-thiadiazole: 73.50 mg), Th-BT-70 (2,5-dibromothiophene: 41.13 mg; 4,7-dibromobenzo[*c*]-1,2,5-thiadiazole: 97.89 mg), Th-BT-90 (2,5-dibromothiophene: 8.06 mg; 4,7-dibromobenzo[*c*]-1,2,5-thiadiazole: 138.17 mg) and Th-BT-100 (4,7-dibromobenzo[*c*]-1,2,5-thiadiazole: 146.99 mg). Triethylamine (2 mL) and an aqueous solution (17 mL) of sodium *n*-dodecylsulfate (200 mg) were added to the organic phase and vigorously stirred using a Branson W-450D digital Sonifier operating at 70% of amplitude for 2 min. The reaction mixture was then stirred and heated at 80 °C overnight. The resulting CMP nanoparticles were transferred to a dialysis tube (MWCO 14 000 Da) with continuous water substitution to remove the surfactant.

Characterization

The UV/Vis absorption spectra were recorded on a Perkin Elmer Lambda 25 UV-Vis spectrometer. FT-IR spectra were recorded on a Nicolet 730 FT-IR spectrometer. ^{1}H-NMR measurements were recorded on a Bruker Avance 250 system. Solid state ^{13}C CP/MAS NMR spectroscopy was taken on a Bruker Avance solid state NMR spectrometer operating at 300 MHz Larmor frequency equipped with a standard 4 mm magic angle spinning (MAS) double resonance probe head. The polymer surface area and pore size distribution were measured *via* nitrogen adsorption and desorption at 77.3 K using an Autosorb-1 (Quantachrome Instruments). The data were evaluated using QuadraWin software from Quantachrome Instruments. Pore size distributions and pore volumes were derived from the adsorption branches of the isotherms using Quenched Solid Density Functional Theory (QSDFT; N_2, assuming carbon adsorbent with slit pores). The samples were degassed at 150 °C for 24 h under vacuum before analysis. The BET surface area calculation was based on data points obtained from $0.05 < P/P_0 < 0.35$ and the nonlinear density functional theory (NLDFT) equilibrium model was used for the BET model fitting. Thermogravimetric analysis (TGA) was performed on a Mettler Toledo TGA-851 system. Sample scans were carried out under nitrogen using a heating rate of 10 °C min^{-1}. Scanning electronic microscopy (SEM) images were acquired on a LEO Gemini 1530 (Carl Zeiss AG, Germany) using an in-lens SE detector. Transmission electronic microscopy (TEM) images were taken on a JEM 1400 (JEOL, USA). Electron paramagnetic resonance (EPR) was measured on a Magnettech Miniscope MS200 spectrometer. Cyclic voltammetry (CV) was recorded on an Autolab potentiostat PGSTAT204 (Metrohm).

Photocatalytic disinfection test

The photocatalytic inactivation of bacteria was conducted using a white LED (1.2 W cm^{-2}, OSA Opto Lights) as a light source. All glass apparatuses used in the experiments were autoclaved at 121 °C for 20 min to ensure sterility. The bacterial cells were cultured in a nutrient broth (Sigma Aldrich) and agitated at 300 rpm for 16 h at 37 °C and 30 °C for *E. coli* K-12 and *B. subtilis*, respectively. The cells were then washed with a sterilized saline solution (0.9% NaCl) and the final cell density was adjusted to about 3.0×10^6 cfu (colony forming units) mL^{-1}. The CMP NP was then added to the cell suspension at a final concentration of 1 mg mL^{-1} and kept in the dark for 60 min to ensure the establishment of an adsorption/desorption equilibrium between the photocatalyst and the bacterial cells. After this period, the reaction mixture was stirred at 25 °C, bubbled with oxygen and irradiated with visible white light for different time intervals. At selected time intervals, aliquots of the sample were collected and serially diluted with the sterilized saline solution. 0.1 mL of the diluted sample was then immediately spread on nutrient agar (Sigma Aldrich) plates and incubated at 37 °C for 16 h to determine the number of viable cells (in cfu). For comparison, two extra control experiments were also conducted: the dark control was carried out with CMP NPs in the absence of light and the light control was carried under visible light irradiation in the absence of

This journal is © The Royal Society of Chemistry 2016

J. Mater. Chem. B, 2016, **4**, 5112–5118 | **5117**

CMP NPs. The survival fraction was determined by dividing the number of cfu of the samples incubated with CMP NPs by the number of the cfu of the control group in the absence of CMP NPs and light. The photocatalytic experiments using radical scavengers were performed similarly to the above photocatalytic disinfection test but with the addition of radical scavengers (ammonium oxalate, TEMP, catalase, $NaNO_3$ and vitamin C), 0.05 mmol L^{-1}, to the reaction mixture. All treated and control experiments were performed in three independent studies.

Photooxidation of α-terpinene

The photooxidation of α-terpinene was performed using a mixture of α-terpinene (0.1 M), Th-BT-100 (1 mg mL^{-1}) and mesitylene (0.1 M) as the internal standard in 10 ml water/acetonitrile (1 : 1). Under an oxygen flow of *ca.* 10 ml min^{-1}, the reaction mixture was stirred at 25 °C and irradiated with visible white light for 2 h. After this, aliquots of the sample were collected and filtered using a syringe filter and the solution was analyzed by ^{1}H-NMR. The $^1O_2$ generation rate was defined as: $R(^1O_2)$ = (obtained amount of ascaridole [mmol])/(weight of Th-BT-100 [g])/(reaction time [s]). A dark control and a degassed sample experiments were carried out in the absence of light and oxygen, respectively.

Acknowledgements

Notes and references

1 C. R. Paula, V. L. J. Krebs, M. E. Auler, L. S. Ruiz, F. E. Matsumoto, E. H. Silva, E. M. A. Diniz and F. A. C. Vaz, *Med. Mycol.*, 2006, **44**, 479–484.

2 P. E. Sudbery, *Nat. Rev. Microbiol.*, 2011, **9**, 737–748.

3 Q. Zhang, G. Lambert, D. Liao, H. Kim, K. Robin, C.-K. Tung, N. Pourmand and R. H. Austin, *Science*, 2011, **333**, 1764–1767.

4 P. A. Smith and F. E. Romesberg, *Nat. Chem. Biol.*, 2007, **3**, 549–556.

5 R. Chait, A. Craney and R. Kishony, *Nature*, 2007, **446**, 668–671.

6 M. Gao, Q. L. Hu, G. X. Feng, N. Tomczak, R. R. Liu, B. G. Xing, B. Z. Tang and B. Liu, *Adv. Healthcare Mater.*, 2015, **4**, 659–663.

7 M. C. DeRosa and R. J. Crutchley, *Coord. Chem. Rev.*, 2002, **233–234**, 351–371.

8 J. Huang, W. Ho and X. Wang, *Chem. Commun.*, 2014, **50**, 4338–4340.

9 X. F. Jiang, L. Yang, P. Liu, X. Li and J. A. Shen, *Colloids Surf., B*, 2010, **79**, 69–74.

10 H. Wang, J. Shen, G. X. Cao, Z. Gai, K. L. Hong, P. R. Debata, P. Banerjee and S. Q. Zhou, *J. Mater. Chem. B*, 2013, **1**, 6225–6234.

11 L.-S. Zhang, K.-H. Wong, H.-Y. Yip, C. Hu, J. C. Yu, C.-Y. Chan and P.-K. Wong, *Environ. Sci. Technol.*, 2010, **44**, 1392–1398.

12 C. Xing, Q. Xu, H. Tang, L. Liu and S. Wang, *J. Am. Chem. Soc.*, 2009, **131**, 13117–13124.

13 H. X. Yuan, B. Wang, F. T. Lv, L. B. Liu and S. Wang, *Adv. Mater.*, 2014, **26**, 6978–6982.

14 C. Zhu, L. Liu, Q. Yang, F. Lv and S. Wang, *Chem. Rev.*, 2012, **112**, 4687–4735.

15 H. Bai, H. Yuan, C. Nie, B. Wang, F. Lv, L. Liu and S. Wang, *Angew. Chem., Int. Ed.*, 2015, **54**, 13208–13213.

16 H. Yuan, Z. Liu, L. Liu, F. Lv, Y. Wang and S. Wang, *Adv. Mater.*, 2014, **26**, 4333–4338.

17 S. Perni, P. Prokopovich, J. Pratten, I. P. Parkin and M. Wilson, *Photochem. Photobiol. Sci.*, 2011, **10**, 712–720.

18 R. J. White, R. Luque, V. L. Budarin, J. H. Clark and D. J. Macquarrie, *Chem. Soc. Rev.*, 2009, **38**, 481–494.

19 J. X. Jiang, F. Su, A. Trewin, C. D. Wood, N. L. Campbell, H. Niu, C. Dickinson, A. Y. Ganin, M. J. Rosseinsky, Y. Z. Khimyak and A. I. Cooper, *Angew. Chem., Int. Ed.*, 2007, **46**, 8574–8578.

20 Y. H. Xu, S. B. Jin, H. Xu, A. Nagai and D. L. Jiang, *Chem. Soc. Rev.*, 2013, **42**, 8012–8031.

21 N. Kang, J. H. Park, K. C. Ko, J. Chun, E. Kim, H. W. Shin, S. M. Lee, H. J. Kim, T. K. Ahn, J. Y. Lee and S. U. Son, *Angew. Chem., Int. Ed.*, 2013, **52**, 6228–6232.

22 F. Vilela, K. Zhang and M. Antonietti, *Energy Environ. Sci.*, 2012, **5**, 7819–7832.

23 Y. Xie, T. T. Wang, X. H. Liu, K. Zou and W. Q. Deng, *Nat. Commun.*, 2013, **4**, 1960.

24 J. X. Jiang, Y. Y. Li, X. F. Wu, J. L. Xiao, D. J. Adams and A. I. Cooper, *Macromolecules*, 2013, **46**, 8779–8783.

25 B. C. Ma, S. Ghasimi, K. Landfester, F. Vilela and K. A. I. Zhang, *J. Mater. Chem. A*, 2015, **3**, 16064–16071.

26 H. Urakami, K. Zhang and F. Vilela, *Chem. Commun.*, 2013, **49**, 2353–2355.

27 Z. J. Wang, S. Ghasimi, K. Landfester and K. A. I. Zhang, *Adv. Mater.*, 2015, **27**, 6265–6270.

28 K. Zhang, D. Kopetzki, P. H. Seeberger, M. Antonietti and F. Vilela, *Angew. Chem., Int. Ed.*, 2013, **52**, 1432–1436.

29 X. Ding and B. H. Han, *Angew. Chem., Int. Ed.*, 2015, **54**, 6536–6539.

30 M. Gruner, L. Tuchscherr, B. Loffler, D. Gonnissen, K. Riehemann, M. C. Staniford, U. Kynast and C. A. Strassert, *ACS Appl. Mater. Interfaces*, 2015, **7**, 20965–20971.

31 A. P. Castano, P. Mroz and M. R. Hamblin, *Nat. Rev. Cancer*, 2006, **6**, 535–545.

32 F. Wang, J. H. Seo, Z. D. Li, A. V. Kvit, Z. Q. Ma and X. D. Wang, *ACS Appl. Mater. Interfaces*, 2014, **6**, 1288–1293.

33 P. Zhang, Z. H. Weng, J. Guo and C. C. Wang, *Chem. Mater.*, 2011, **23**, 5243–5249.

34 Y. Chen, J. S. Zhang, M. W. Zhang and X. C. Wang, *Chem. Sci.*, 2013, **4**, 3244–3248.

35 Y. J. Cui, Z. X. Ding, P. Liu, M. Antonietti, X. Z. Fu and X. C. Wang, *Phys. Chem. Chem. Phys.*, 2012, **14**, 1455–1462.

36 M. N. Chong, B. Jin, C. W. K. Chow and C. Saint, *Water Res.*, 2010, **44**, 2997–3027.

37 A. Markowska-Szczupak, K. Ulfig and A. W. Morawski, *Catal. Today*, 2011, **169**, 249–257.

38 D. R. Kearns, *Chem. Rev.*, 1971, **71**, 395–427.

39 M. C. DeRosa and R. J. Crutchley, *Coord. Chem. Rev.*, 2002, **233**, 351–371.